

LOI for proposal to construct instrumentation that will enable novel science with the LCLS (category C).

Wavelength Dispersive Optics for Ultrafast X-ray Spectroscopy at LCLS

Uwe Bergmann

Stanford Synchrotron Radiation Laboratory

Menlo Park, California 94025

e-mail: bergmann@slac.stanford.edu, ph: +1 650 926 3048, fax: +1 650 926 4100

Ultrafast X-ray absorption spectroscopy (XAS) performed at an x-ray free electron laser (XFEL) is a potentially very powerful tool to study numerous phenomena including dissociation in the gas phase ¹, phase transitions in material science ² and metal ligand charge transfer reactions ³ in coordination chemistry (for a recent review see ⁴). At energies of 5-8 keV the LCLS is expected to provide pulses of order 10^{12} photons within an energy band pass of < 8 eV. Such a band pass is not sufficient to perform single shot XAS, which requires > 30 eV for XANES and several hundred eV for EXAFS. In pump-probe experiments, using many pulses, it will in principle be possible to quickly vary the LINAC energy to provide a larger spectral range. But this approach is very challenging with regards to systematical errors inherent to XFEL radiation, most notably variations in pulse intensity, pulse energy distribution and time jitter.

Inelastic X-ray Raman scattering (XRS) and x-ray emission spectroscopy (XES) are techniques that provide spectroscopic information of the local structure and local electronic structure without the requirement of a wide incident band pass. With a wavelength dispersive analyzer system of sufficient solid angle such spectra can, in some cases, be obtained from a single shot. When many shots are required for sufficient statistics, the method has the benefit that systematical errors are minimized because in each shot a complete spectrum is recorded. Here we propose to develop and test x-ray instrumentation to carry out such spectroscopic studies at LCLS.

X-ray emission spectroscopy

It has long been known that the x-ray emission spectrum contains detailed chemical and structural information ⁵. In particular the 5-8 keV range is very attractive, since it includes K-emission lines of most 3d transition metals and L-lines of several rare earths. Furthermore perfect crystal Bragg optics is well suited for this energy range and the hard x-ray probe is sufficiently penetrating to enable a number of sample conditions and environments.

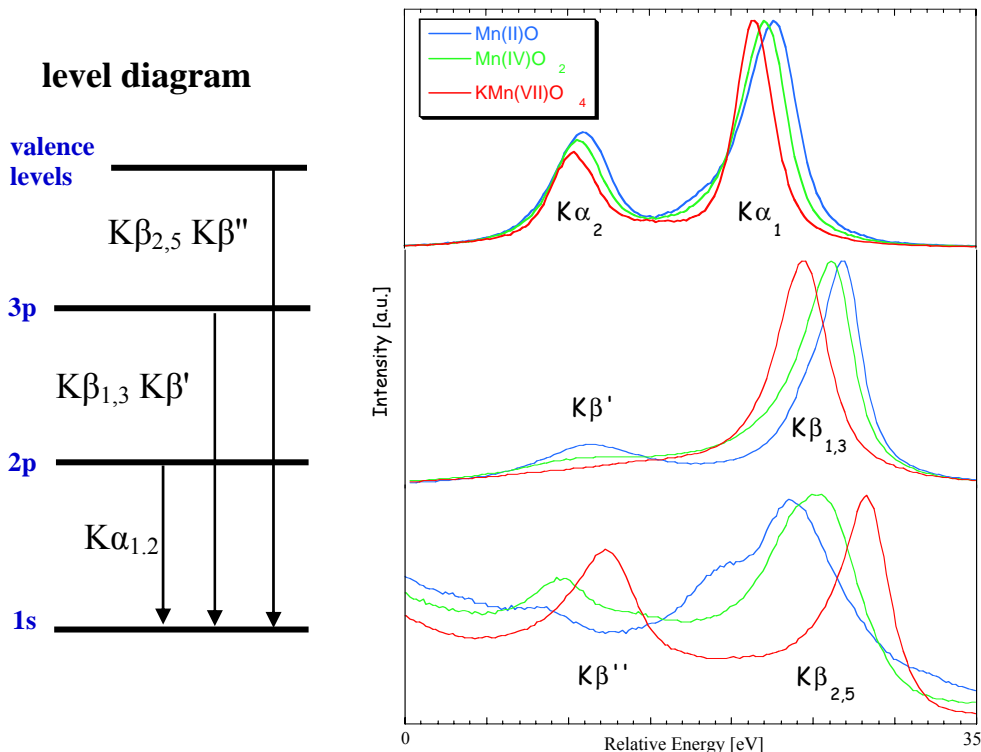


Fig 1: Level diagram and complete K emission spectra for Mn oxides. Intensities of different levels are scaled arbitrarily.

Figure 1 shows the complete K XES for Mn oxides to illustrate the information content in the various parts of the spectrum. Using a 1s hole excited initial state, K emission probes the *occupied* p-density of states, as compared to K XANES, which probes the *unoccupied* p-density of states. Least affected by the chemical environment of the absorbing metal atom is the 2p-1s $K\alpha$ spectrum. Large changes in oxidation state still give rise to a small spectral change (peak width and energy) due to 2p-3d exchange interaction. The $K\beta_{1,3}$ main peak (2p – 1s) shows somewhat larger spectral shifts resulting from the 3p-3d exchange interaction. These shifts have been used to study small changes in oxidation state at the active Mn site in the very important metalloprotein photosystem II^{6, 7}. From systematic studies on model compounds it was found that, compared to XANES, the $K\beta_{1,3}$ shifts are more linearly correlated with the oxidation state and depend less on structure^{8, 9}. The $K\beta_{1,3}$ main line is very well sensitive also to the spin state because its peak position is directly dependent on the number of unpaired 3d electrons. This has been applied in a recent study of Fe partitioning in the mantle of Earth¹⁰.

Transitions from valence levels are known as $K\beta''$ and $K\beta_{2,5}$, and particularly the $K\beta''$ so-called cross-over transitions contain unique information on ligand type and distance¹¹. In the example shown in Figure 1 the $K\beta''$ peaks result from O 2s to Mn 1s transitions. Both their intensities and energies change significantly for the different oxides. As has been shown in¹¹ the integrated $K\beta''$ peak intensity scales logarithmically with the Mn-O distance and the energy changes with the charge on the Mn. Furthermore, different ligands such as e.g. N, O and F can be distinguished by an even larger energy shift reflecting their different 2s binding energies. Hence,

the $K\beta''$ spectrum is a very powerful direct probe to study e.g. the dissociation or interchange of ligands.

Non-Resonant X-ray Raman Scattering (XRS)

Light-atom XANES spectra are commonly measured in transmission, Auger yield, electron yield, sample photocurrent or fluorescence excitation modes¹². Each method has its advantages and limitations. Due to the submicron path lengths of soft x-rays, transmission measurements require very thin samples that are sometimes difficult to prepare. The samples should also be transversely homogeneous, and limited sensitivity restricts experiments to relatively concentrated systems. To simplify sample preparation, the various electron detection methods are often employed. However, these methods have probe depths of less than 50 Å and are thus surface sensitive¹³. In fact, they might provide information about an oxide coating or sorbed atoms rather than about the bulk sample. Fluorescence yield probes deeper into the sample, but it can suffer from artifacts due to ‘saturation effects’ in concentrated systems¹⁴ or from variations in fluorescence yield across the absorption edge¹⁵. These considerations show that there is a large class of systems and experimental conditions where the bulk properties are difficult to probe by conventional XANES methods. This class includes heterogeneous concentrated compounds, reactive materials, liquids, and systems under extreme pressure or temperature. Higher energy x-ray probes have several advantages for such samples, including ‘bulk’ sensitivity and less stringent requirements on the sample environment. Equipment such as flow tubes, furnaces, *in situ* chambers and high-pressure cells has all been employed in the 5-8 keV range.

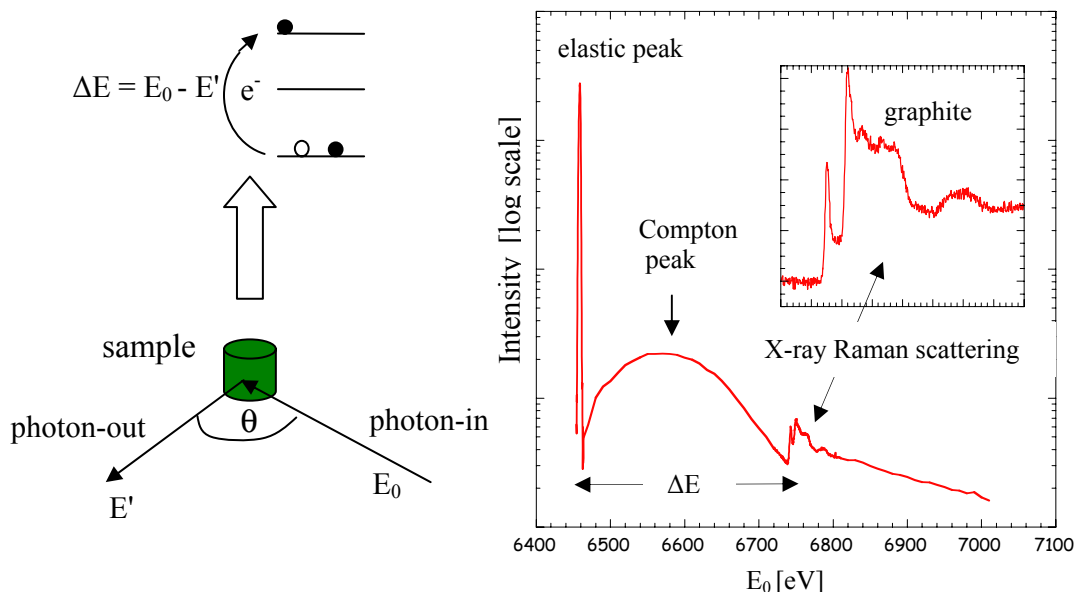


Fig. 2 Left: Concept of XRS. The energy transfer from an inelastically scattered photon results in the excitation of a core electron into an empty state. Right: Complete scattering spectrum from graphite. Intensity versus incident energy E_0 is plotted, analyzer energy E' is fixed at 6460 eV.

X-ray Raman scattering (XRS) is a technique that can retain all of the experimental advantages of hard x-ray measurements, while revealing the information provided by soft x-ray absorption spectroscopy. In XRS, a photon with energy E_0 is inelastically scattered with energy E' and the lost energy results in the excitation of a core electron. By measuring the energies of both the incident (E_0) and scattered photon (E') one can obtain the energy transfer $\Delta E = E_0 - E'$ that corresponds now to the excitation energy in conventional XAS. Varying ΔE can be accomplished by either changing the incident monochromator energy, or by changing the analyzer energy. The latter provides the crucial advantage for an LCLS based experiment, because it does not require a large incident energy band pass. In the proposed setup, variation of the analyzer energy is achieved with wavelength dispersive optics and a 1 or 2 dimensional position sensitive detector (PSD).

Figure 2 shows the full photon-in photon-out spectrum of a graphite sample using 6-7 keV x-rays. Here the incident energy E_0 is varied, but a basically identical mirror imaged spectrum is obtained when varying E' . At $\Delta E = 0$ is quasi-elastic peak is seen, then a broad Compton peak and finally the XRS spectrum showing typical XANES features of graphite. It has long been known that at low momentum transfer q , the matrix element is the same for both XRS and XAS^{16, 17}. When q is large, non-dipole transitions become allowed in XRS and density of states with other than p character can be probed in a K edge experiment^{18, 19}. What has limited XRS in the past is the very small scattering cross section, but with powerful new synchrotron sources and new analyzer instrumentation several XRS based studies have been reported recently (see e.g.²⁰⁻²³). Especially the work on water has caught considerable attention, and XRS, which can be performed throughout the whole complex phase diagram of this unique system, is expected to play a major role in future studies. In fact, very recently high quality EXAFS²⁴ and XANES on supercritical water²⁵ were obtained with XRS.

The XRS signal is proportional to Z^4 (Z = electrons per scatterer) and current studies have focused on low Z materials. However, from the XRS counting rates now observed we estimate that with an efficient instrument all elements in the periodic table up to 3d transition metals (at higher Z one would use L and M edges) can be studied. XRS L and M-edge spectra of Sc have been first reported by Caliebe²⁶.

Concept of instrumentation and some numbers

Different types of wavelength dispersive devices can be envisioned and in the proposed work more than one will be tested. Here we briefly discuss a concept based on arrays of cylindrically curved analyzers and a PSD²⁷. Sagittal focusing of a cylindrically curved analyzer (as compared to e.g. a spherical curved device) has only a second-order effect on its energy resolution and is therefore well suited in a wavelength dispersive device with good energy resolution. Figure 3 shows the schematics of a possible design. Each of the four quarter-circles consists of several crystals, with a radius of curvature of order 30 cm (depending on the required resolution). The solid angle Ω of such a device can be calculated with the following equation:

$$\Omega[4\pi \text{ sr}] = 1/2 [\cos\theta - \cos(\theta - \Delta\theta)] \approx 1/2 \Delta E/E \sin\theta \tan\theta$$

Here Ω is expressed as a fraction of 4π sr. Using, e.g., a Si(444) reflection (backscattering energy = 7.9 keV) the Bragg angles in the XANES region (~ 100 eV) can range from 81° to 88° and the total solid angle would be 6% of 4π sr. At an energy resolution of $\Delta E = 0.5$ eV, the solid angle per ΔE ranges from $2 \cdot 10^{-4}$ at 81° to $9 \cdot 10^{-4}$ at 88° . In favorable cases, such as e.g. H₂O, this results in an XRS signal of ~ 10 photons/bunch/ ΔE or $\sim 10^3$ photons/bunch/spectrum. A good XANES spectrum would require $\sim 10^3$ bunches.

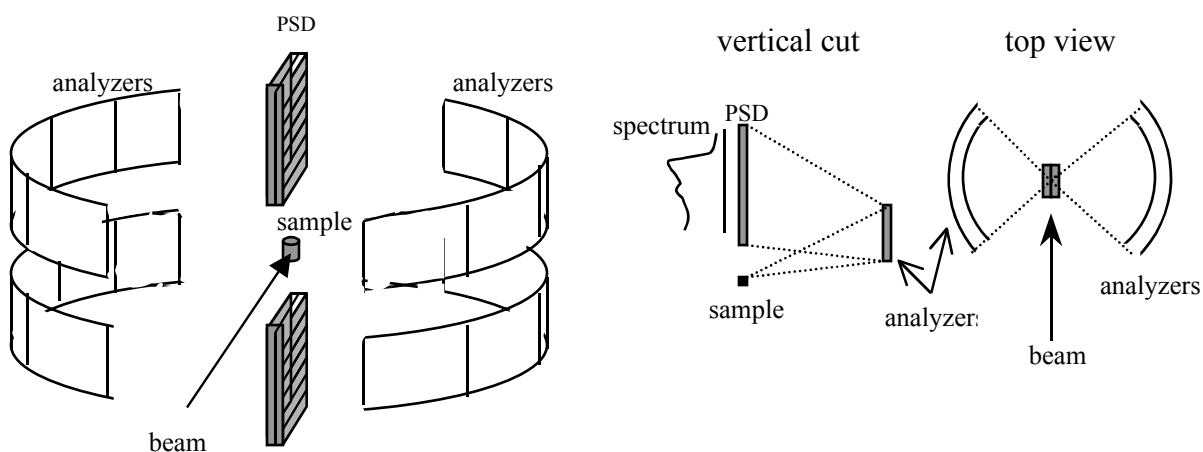


Figure 3 Schematic setup four arrays of cylindrically curved crystals in sagittal focusing mode. Scattering of a point source beam is analyzed at different energies (see vertical cut) resulting in a spectrum on the PSDs. For XRS the setup is rotated by 90° for scattering in the predominantly vertical plane.

In EXAFS experiments the maximal energy range is ~ 800 eV (corresponding to $k < 14 \text{ \AA}^{-1}$ with a 50 eV pre-edge region). The range of Bragg angles in this case is $65^\circ - 88^\circ$ resulting in a total solid angle of 19% of 4π sr. With an energy resolution of $\Delta E = 10$ eV, the solid angle per ΔE ranges from $1.1 \cdot 10^{-3}$ at 65° to $1.8 \cdot 10^{-2}$ at 88° . The incident photon flux would be essentially the total number of photons i.e. $\sim 10^{12}$ /bunch resulting in an EXAFS signal of $\sim 10^2 - 10^3$ photons/bunch/ ΔE . With $10^3 - 10^4$ bunches a good EXAFS spectrum can be obtained.

For XES measurements on e.g. concentrated 3d transition metal compounds we estimate that the $K\beta_{1,3}$ spectrum (spin/oxidation state) can be obtained from a single bunch and the $K\beta''$ spectrum (ligand dissociation) from $\sim 10^3$ bunches.

Summary

Two techniques that open the possibility to carry out ultrafast x-ray spectroscopy at LCLS were introduced. The concept of wavelength dispersive instrumentation to realize such studies was discussed and some estimates of expected signal count rates were presented. It is important to note that, in principle, the technology is available now to build both the crystal analyzers and the PSD. In fact, a prototype system that is conceptionally similar to the one described here has already been applied for XES studies²⁸. R&D work of an optimized system can be performed at existing synchrotron facilities, and a device could be ready in time to take full advantage of the unique properties of LCLS.

References

- 1 F. Raksi, K. R. Wilson, Z. M. Jiang, et al., J. Chem. Phys. **104**, 6066 (1996).
2 S. L. Johnson, P. A. Heimann, A. M. Lindenberg, et al., Physical Review Letters **91**,
157403 (2003).
3 M. Saes, C. Bressler, R. Abela, et al., Physical Review Letters **90**, 047403 (2003).
4 C. Bressler and M. Chergui, Chem. Rev. **104**, 1781 (2004).
5 A. Meisel, G. Leonhardt, and R. Szargan, *X-Ray Spectra and Chemical Binding*
(Springer-Verlag, New York, 1989).
6 U. Bergmann, M. M. Grush, C. R. Horne, et al., Journal of Physical Chemistry B **102**,
8350 (1998).
7 J. Messinger, J. H. Robblee, U. Bergmann, et al., Journal of the American Chemical
Society **123**, 7804 (2001).
8 H. Visser, E. Anxolabehere-Mallart, U. Bergmann, et al., J Am Chem Soc **123**, 7031
(2001).
9 S. A. Pizarro, P. Glatzel, H. Visser, et al., Physical Chemistry Chemical Physics
submitted (2004).
10 J. Badro, G. Fiquet, F. Guyot, et al., Science **300**, 789 (2003).
11 U. Bergmann, C. R. Horne, T. J. Collins, et al., Chem. Phys. Lett. **302**, 119 (1999).
12 J. Stöhr, *NEXAFS spectroscopy* (Springer-Verlag, Berlin ; New York, 1992).
13 M. Abbate, J. B. Goedkopp, F. M. F. de Groot, et al., Surface Interface Anal. **18**, 65
(1992).
14 J. Goulon, C. Goulon-Ginet, R. Cortes, et al., Journal de Physique **43**, 539 (1982).
15 F. M. F. deGroot, M.-A. Arrio, P. Saintavit, et al., Physica B **208-209**, 84 (1995).
16 Y. Mizuno and Y. Ohmura, Journal of the Physical Society of Japan **22**, 445 (1967).
17 T. Suzuki, Journal of the Physical Society of Japan **22**, 1139 (1967).
18 C. Sternemann, M. Volmer, J. A. Soininen, et al., Physical Review B **68** (2003).
19 M. H. Krisch, F. Sette, C. Masciovecchio, et al., Physical Review Letters **78**, 2843
(1997).
20 U. Bergmann, P. Wernet, P. Glatzel, et al., Physical Review B **66**, 092107 (2002).
21 U. Bergmann, H. Groenzin, O. C. Mullins, et al., Chemical Physics Letters **369**, 184
(2003).
22 M. L. Gordon, D. Tulumello, G. Cooper, et al., Journal of Physical Chemistry A **107**,
8512 (2003).
23 P. Wernet, D. Nordlund, U. Bergmann, et al., Science **304**, 995 (2004).
24 U. Bergmann, A. Nilsson, P. Wernet, et al., unpublished (2004).
25 P. Wernet, D. Testemale, J.-L. Hazemann, et al., submitted (2004).
26 W. A. Caliebe, Ph.D. thesis in Physics (University of Kiel, Germany, Kiel, 1997).
27 U. Bergmann and R. Frahm, TDR XFEL workshop series "Methods and Instrumentation
for the XFEL", J. Hastings and Th. Tschentscher, eds., 52 (2001).
28 Y. Udagawa, private communication.